http://dx.doi.org/10.5012/bkcs.2013.34.8.2473

Reaction Dynamics of CH_3 + HBr → CH_4 + Br at 150-1000 K

Jongbaik Ree,[*] Yoo Hang Kim,[†] and Hyung Kyu Shin[‡]

Department of Chemistry Education, Chonnam National University, Gwangju 500-757, Korea. [*]E-mail: jbree@jnu.ac.kr
[†]Department of Chemistry, Inha University, Incheon 402-751, Korea
[‡]Department of Chemistry, University of Nevada, Reno, Nevada 89557, USA
Received May 9, 2013, Accepted May 30, 2013

The kinetics of the radical-polar molecule reaction CH_3 + HBr → CH_4 + Br has been studied at temperatures between 150 and 1000 K using classical dynamics procedures. Potential energy surfaces constructed using analytical forms of inter- and intramolecular interaction energies show a shallow well and barrier in the entrance channel, which affect the collision dynamics at low temperatures. Different collision models are used to distinguish the reaction occurring at low- and high-temperature regions. The reaction proceeds rapidly *via* a complex-mode mechanism below room temperature showing strong negative temperature dependence, where the effects of molecular attraction, H-atom tunneling and recrossing of collision complexes are found to be important. The temperature dependence of the rate constant between 400 and 1000 K is positive, the values increasing in accordance with the increase of the mean speed of collision. The rate constant varies from 7.6×10^{-12} at 150 K to 3.7×10^{-12} at 1000 K *via* a minimum value of 2.5×10^{-12} cm^3 molecule^{-1} s^{-1} at 400 K.

Key Words : Complex-mode reaction, Tunneling, Trajectory, Rate constant

Introduction

Reactions of alkyl radicals with hydrogen halides have been a subject of active studying for several decades, producing wealth of information on their kinetics and thermochemistry. Interest in these and related reactions is due in part to the usefulness of their data in thermochemical studies and developing further studies involving free radicals.[1-18] The common characteristics of these reactions are the abstraction of a hydrogen atom by a radical in a highly exo-ergic environment with a low or negligible activation energy barrier and rate constants showing weak temperature dependence.[7,10,12-14,17,18] A particularly significant aspect of the temperature dependence is that some simple reactions involving radicals proceed *via* negative activation energies at low temperatures (< 500 K).[7,12-14,17,18] One such reaction is CH_3 + HBr → CH_4 + Br, which is a prototypical system for free radical reactions and the subject of the present paper. In recent years, chemical reactions involving bromine and its derivatives such as HBr, BrO, HOBr and CH_3Br have become an important subject in studying the delicate balance of atmospheric molecules and atoms, in particular those in the Arctic polar region,[19-23] even though their concentrations are low. Bromine atom produced in the CH_3 + HBr reaction undergoes many reactions with various molecules in the atmosphere, such as the ozone depletion reaction O_3 + Br → BrO + O_2, where BrO regenerates Br either by photolysis at ~325 nm or by reaction with NO. Hydrogen bromide enters the atmosphere by a variety of industrial, natural and anthropogenic processes, such as coal-burning, mineral industries, waste combustion, oceanic biological processes and reactions of acidic gases with sea salt. Earlier reports indicate about 700 metric tons of HBr were released to atmosphere in 2002.[24] One of the sources of bromine formation is the CH_3 + HBr reaction, where the reactivity can be greatly influenced by the attractive interaction of a free radical with a polar molecule especially at low temperatures prevailing in the atmospheric environment.

In this study, we report the temperature dependence of CH_3 + HBr → CH_4 + Br with emphasis on the low temperature range (< 300 K) of the atmospheric environment based on a complex-mode model which uses collision trajectories radically different from those of high-temperature gas-phase reactions. We will consider the effects of free radical-polar molecule attraction, H-atom tunneling through a transition-state barrier and recrossing of the nascent complex formed in the interaction of CH_3 and HBr in detail. The reaction will be extended to higher temperatures (300-1000 K) to study how the magnitudes and temperature dependence of the rate constants differ from those of the complex-mode rate constants at low temperatures. We use a molecular dynamics approach to solve the equations of motion for the potential energy composed of the analytical expressions of inter- and intramolecular interactions.

Model and Methods

The collision model is similar to that used for CH_3 + OH in ref. 25. We recapitulate the essential aspects here defining all coordinates in Figure 1. The center-of-mass (c.m.) of HBr is taken to be the origin of the XYZ frame and planar CH_3 approaches at the impact parameter b with the collision energy E. The potential energy U used for the CH_3 + HBr interaction includes the exponential C-H and C-Br intermolecular terms (Morse-type), H-Br intramolecular interactions, intermolecular terms between H of HBr and three

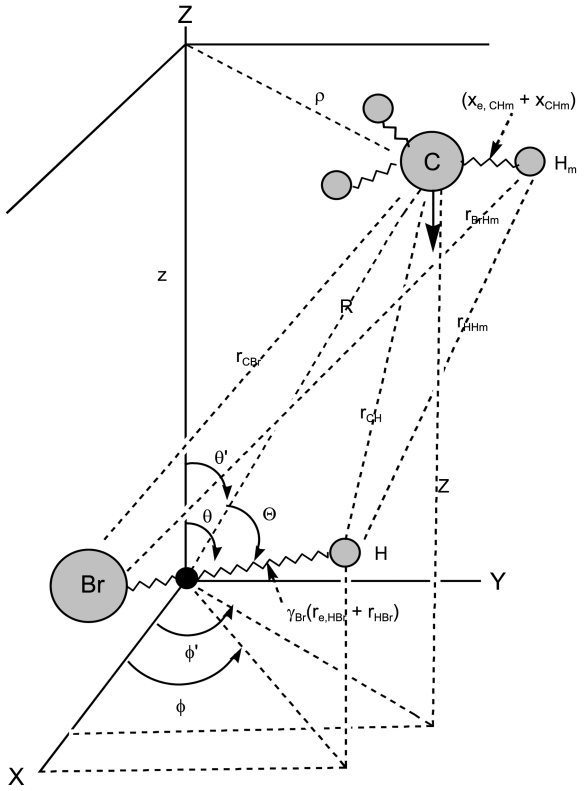

Figure 1. Model for the collision of CH_3 with HBr. The distances from only one H of CH_3 are shown; see H_m. The capital letter Z stands for the Z axis, whereas the lower-case z measures the vertical distance between C and the XY plane.

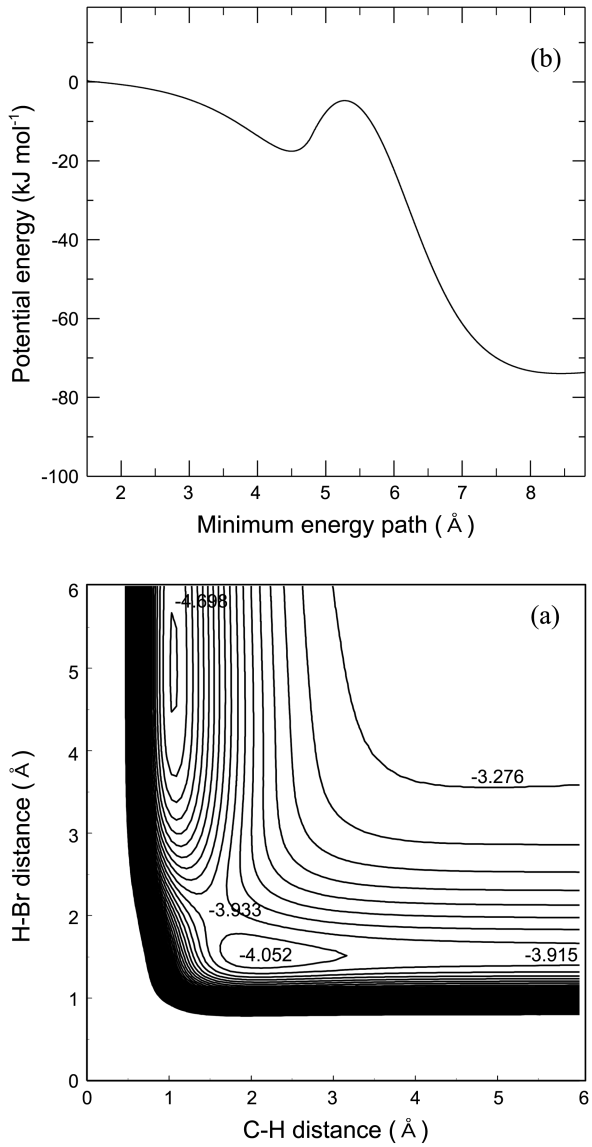

Figure 2. (a) Representative potential energy surface for a near-collinear orientation $H_3C\cdots$H-Br with θ = 80°, Θ = 9° and b = 0. Energies are in eV and the energy spacing is 0.043 eV. The exit valley minimum occurs at –4.698 eV. (b) Minimum energy path on the kJ scale. The barrier height measured from the well bottom is 11.45 kJ. kJ units are used to compare with thermochemical data.

hydrogen atoms of the methyl radical (H-H_m), the same forms between Br and three H_m atoms, and three C-H_m intramolecular terms in CH_3. The electrostatic and induction part includes contributions from charge-dipole, charge-induced dipole, and dipole-induced dipole interactions, which contribute to the approach of the reactants to close separations of each other. The time-evolution of the relative distance R between the centers of mass of CH_3 and HBr determines the collision trajectory. The complete form of the interaction potential is given in the Appendix.

A representative case of the potential energy surface (PES) determined from the potential function given in the appendix is shown in Figure 2(a). The entrance valley is relatively flat and shows a barrier near r_{CH} = 1.6 Å and r_{HBr} = 2.0 Å, beyond a basin of depth 0.137 eV (13.2 kJ mol^{-1}). The valley drops steeply to a minimum in the exit valley, where the CH bond forms and Br recedes from H. The product CH_4 travels through a narrow exit valley with a significant amount of vibrational energy in its nascent CH bond (see the next section). These events follow the minimum energy path shown in Figure 2(b), where the reactants enter the entrance channel which slowly declines to a potential well before rising to a barrier. The path then falls off to −75.5 kJ mol^{-1}, which is close to the thermochemical value ΔH^o = −74 kJ mol^{-1},[6,26] in an exo-ergic reaction. (Here the entrance energy is set zero and scaled in the kJ units for easy comparison with the thermochemical data.) The shallow well in the entrance valley can trap low energy reactants in the form of a weakly bound complex $H_3C\cdots$HBr. The complex can reach the product state when H-atom of HBr tunnel through the barrier and binds the radical, the tunneling efficiency increasing when the temperature is lowered. Others can return to the reactant state at a faster rate than going on to the product state, thus reducing the extent of forward events.

Tunneling has been an important part of studying reaction rates involving small particles which can pass through the potential energy barrier.[14,20,27-32] Although tunneling by atoms heavier than hydrogen are considered to be rare, recent studies show atoms as heavy as carbon can tunnel through the reaction barrier at cryogenic temperatures.[33-35] The extent of H-tunneling in the present reaction can be determined by

use of the WKB expression[36]

$$\chi(T) = \frac{1}{k_B T} e^{V_o/k_B T} \int_0^{V_0} \left[\exp\left\{ -(2/\hbar)(2m_H)^{1/2} \int_{R_1}^{R_2} [V_{TS}(R_{MEP}) - E_H]^{1/2} dR_{MEP} \right\} \right] e^{-E_H/k_B T} dE_H , \quad (1)$$

where $V_{TS}(R_{MEP})$ is the potential energy of the transition state barrier above the well minimum, R_1 and R_2 are the inner and outer turning points along the minimum energy path (MEP), respectively, and E_H is the translational energy of the H atom. The upper limit of the outer integration is set as the barrier height and the value of $\chi(T)$ is 1 for $E_H > V_o$. The potential energy can be closely fit to the quadratic form: $V_{TS}(R_{MEP}) = 11.47 - 0.0687R_{MEP} - 32.62R_{MEP}^2$ kJ mol^{-1} around the barrier maximum. The function yields the absolute value of the imaginary frequency of the barrier $\nu_{TS} = 120$ cm^{-1}, or 1.4 kJ mol^{-1}. The calculated value of $\chi(T)$ is 1.48 at 300 K and decreases to 1.08 at 1000 K. At 200 K, it is 1.95 and it is as high as 2.86 at 150 K, thus significantly affecting the extent of reaction at lower temperatures.

To follow the time evolution of reactive events, we solve the equations of motion for the Hamiltonian *H* containing the coordinates in U and their conjugated momenta in the kinetic energy terms:

$$\dot{q}_n = \partial H/\partial p_n, \; \dot{p}_n = -\partial H/\partial q_n, \quad (2)$$

where *n* denotes R, r_{HBr}, θ, ϕ, ρ, x_{CHm_i}. Here ρ is the distance from the c.m. of CH_3 to the Z axis and its initial value is the impact parameter *b* and x_{CHm_i} is the displacement of the *i*th CH_m bond from its equilibrium distance. The orientation angle is $\Theta = \cos^{-1}[\cos\theta\cos\theta' + \sin\theta\sin\theta'\cos(\phi - \phi')]$, where $\cos\theta' = z/R$, $\sin\theta' = \rho/R$, $R = (\rho^2 + z^2)^{1/2}$. The atom-atom distances r_{CH} and r_{CBr} are determined in terms of R, r_{HBr} and Θ; see Eq. (A2). We sample the collision energy E at each temperature using the Maxwell-Boltzmann distribution and use standard numerical routines[37] based on Adams-Moulton's method to integrate the equations of motion. We start computations for 40 000 sets of randomly sampled initial conditions. The integration step size is taken to be 0.10 fs. The collision dynamics are followed when CH_3 reaches HBr at R ≈ 15 Å from a long distance. The conditions of HBr bond dissociation are set when the bond distance reaches 5 Å and the bond energy reaches the dissociation threshold D_{HBr}. Similarly, CH bond formation is determined when the bond distance and energy become less than 5 Å and the dissociation threshold, respectively.

Of the initial conditions, those describing the approach of collision partners from a long distance are particularly important in the present study as they have different forms depending whether the collision occurs at low or high temperatures (or low or high collision energies). For collisions taking place at or above room temperature, the initial conditions for the relative motion at a large distance described by $U(R) = D[e^{(Re-R)/a} - 2e^{(Re-R)/2a}]$ is[38]

$$R(t_o) = R_e + a\ln(\rho^2 + \rho) + 2a\ln\{\cosh[(E/2\mu)^{1/2} t_o/a] - [\rho/(1+\rho)]^{1/2}\} \quad (3a)$$

$$p(t_o) = 2(E/2\mu)^{1/2}\sinh[(E/2\mu)^{1/2}t_o/a]\{\cosh[(E/2\mu)^{1/2}t_o/a] - [\rho/(1+\rho)]^{1/2}\}^{-1} \quad (3b)$$

where ρ = D/E and μ is the reduced mass of the collision system. The potential parameters D and R_e needed to initialize at long distance are 0.0211 eV and 4.04 Å obtained from the Lennard-Jones constants $\sigma_{CH_3} = 3.80$ Å, $\varepsilon_{CH_3}/k_B = 144.0$ K[39] and $\sigma_{HBr} = 3.41$ Å, $\varepsilon_{HBr}/k_B = 417$ K.[40] The exponential range parameter *a* is obtained from[41] $a = \pi^{-1/2}[\Gamma(7/12)/\Gamma(1/12)][½(\sigma_{CH_3} + \sigma_{HBr})](4D/kT)^{1/12} = 0.298$ Å at 300 K. All other spectroscopic and potential constants are given in Table 1. However, at lower temperatures, where the strength of molecular attraction is significant, the reactants can form a collision complex as they travel toward the barrier. Statistically they spend more time along the reaction path where attraction is strong. During the journey through the region of potential well, the intermolecular distance R does not change significantly, so that we can expand the interaction potential around the well bottom R_o: $U(\theta,\phi) = U(\theta,\phi)_o + ½|\partial^2 U(\theta,\phi)/\partial R^2|_o(R - R_o)^2 + \cdots$ for $r_{HBr} = r_{HBr,e}$. The angle dependence of charge-dipole and dipole-induced dipole interaction energies is simple, but together with the angular dependence of intermolecular atom-atom distances, it controls the motion of reactants in the entrance valley. For the weakly bound complex travelling in the region of the potential well, the potential energy is the angle-averaged quantity

$$<U> = \frac{\int_0^{2\pi}\int_0^{\pi} \{U(\theta,\phi)\exp[-U(\theta,\phi)/k_B T]\}\sin\theta d\theta d\phi}{\int_0^{2\pi}\int_0^{\pi} \exp[-U(\theta,\phi)/k_B T]\sin\theta d\theta d\phi} \quad (4)$$

where the Boltzmann weighting factor is introduced as the complex spends more time at orientations where the energy is more attractive. The resulting average up to the second order is $<U> = <U_o> + ½<U">(R - R_o)^2$, where the angle-averaged second derivative <U"> is evaluated at $R = R_o$. From the solution of the equation of motion for the quadratic function the initial conditions appropriate for the reaction at low temperatures are

Table 1. Spectroscopic and Potential Constants

	HBr	CH in CH_4	CBr in CH_3Br	CH_m in CH_3	HH_m
D (eV)	3.922[a]	4.587[c]	2.94[c,d]	5.10[c]	4.751[a]
ν (cm^{-1})	2649[a]	2916 (ν_1)[b,c]	611 (ν_3)[c,b]	3270 (ν_1)[f]	4401[a]
a (Å)	0.276	0.278	0.291	0.264	0.257[a]
r_e (Å)	1.414[a]	1.094[c]	1.939[c,d]	1.079[c]	0.741[a]

$D = D_o + ½\hbar\omega$; $a = (D/\mu)^{½}/\omega$. $\mu_{HBr} = 0.827$ debye;[42] $\alpha_{CH_3} = 2.222$ Å,[43] $\alpha_{HBr} = 3.51$ Å.[44] [a]Ref. 45, [b]Ref. 46, [c]Ref. 47, [d]Ref. 48, [e]Ref. 49, [f]Ref. 50.

$$R(t_o) = R_e + [2(E - <U_o>)/|<U">|]^{½}\cos[(<U">/\mu)^{½}t_o], \quad (5a)$$

$$p(t_o) = -[2\mu(E - <U_o>)]^{½}\sin[(<U">/\mu)^{½}t_o]. \quad (5b)$$

At each impact parameter b there exists a probability P(b) that a reactive event will occur. To calculate rate constants we set the maximum impact parameter b_{max} = 10 Å, which is determined from preliminary runs for P(b). The reaction cross section σ(E) is then the integral $2\pi\int_0^{b_{max}} bP(b)db$, which is equivalent to $\sigma(E) = 2\pi\Sigma_0^{b_{max}}\{N_R(b)/N(b)\}b\Delta b$, N($b$) and $N_R(b)$ being the numbers of total and reactive trajectories in a subdivided interval Δb between 0 and b_{max}, respectively. Including the effects of H-atom tunneling discussed above, the rate constant then can be written as

$$k = \chi(T)(8k_BT/\pi\mu)^{½}\int_{E_0}^{\infty}\sigma(E)\,e^{-E/k_BT}(E/k_BT)(dE/k_BT). \quad (6)$$

Alternatively, we can calculate σ(T) using E from the Maxwell-Boltzmann distribution at T and initial vibrational and rotational energies determined from thermal distributions. Then the rate constant can be given as $k = \chi(T)(8k_BT/\pi\mu)^{½}\sigma(T)$.

Results and Discussion

In this section we first consider the dynamics of the reaction. The time evolution of collision events for a representative trajectory at 300 K is shown in Figure 3(a), where we plot the C-H and H-Br distances and collision trajectory R initiated by Eqs. (3a) and (3b). Reaction time is scaled so that the instant of the first impact is zero. The time-variation of collision trajectory and atom-atom distances is simple and indicates the reaction is a short-time event or a direct-mode mechanism. The well-organized oscillation of C-H distance indicates the formation of a nascent bond immediately after the impact. The H-Br distance diverges (or bond dissociation) on impact, describing the time evolution of the Br position from H which is now bound to the methyl radical. The oscillatory structure of the outgoing H-Br distance is due to the vibration of the nascent CH bond, where the alternation of downward and upward oscillations reflects the rotation of CH_4. Similarly, after the impact, the collision trajectory is now the distance between the outgoing Br and C of CH_4. The time evolution of reactive events at higher temperatures follows the same pattern shown in Figure 3(a).

The time evolution of reactive events at lower temperatures (< 300 K) is markedly different from that shown in Figure 3(a). We take a representative reactive event at 200 K and show its time evolution initiated by the conditions given by Eqs. (5a) and (5b) in Figure 3(b). (Note that both Figures 3(a) and 3(b) are plotted on the same scales.) The collision trajectory now progresses with large amplitudes beyond the initial impact. Reaction time passes more than 0.7 ps after the initial impact before the nascent CH bond forms, the duration representing the lifetime of collision complex. The time dependence of the collision trajectory, C-H and H-Br distances clearly indicates the reactive event follows a complex-mode mechanism, where the lifetime of complex far exceeds the period of either HBr or CH vibration. The lifetime is more than 60 times the ν_1 CH vibrational period.

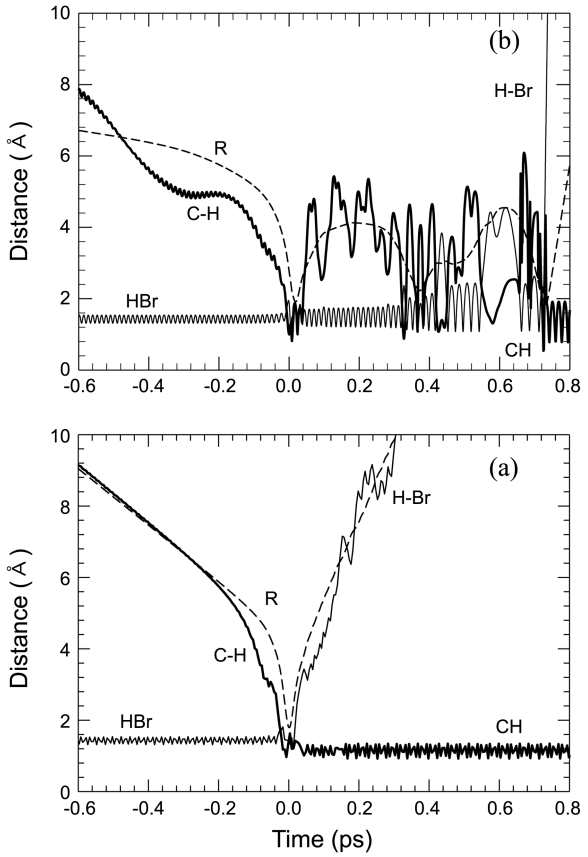

Figure 3. Time evolution of the collision trajectory R, CH distance, and HBr distance for a trajectory representing (a) the direct-mode reaction at 300 K and (b) the complex-mode reaction at 200 K.

From the standpoint of bond dissociation dynamics, the time dependence of H-Br distance shown in Figure 3(b) is particularly interesting as it illustrates the nature of vibrational excitation in the dynamic process. The amplitude of HBr vibration changes gradually from the instant of the initial impact to ~0.7 ps, indicating the excitation of the ground-state reactant HBr toward the dissociation threshold occurs in a series of steps, the HBr bond gaining a small amount of energy at each step. In the direct-mode mechanism at higher temperatures, where the reaction occurs in a strong collision transferring a large amount of energy to the HBr bond, the dynamics is simple as shown in Figure 3(a).

Figure 4(a) shows the relationship between the vibrational energy and bond distance of CH at the instant when the bond is formed. As the bond energy is calculated with the exponential function given in Eq. (A1), the points in the plot are distributed within an envelope of the Morse-type curve. High concentration of the points at low-lying region indicates the vibrational excitation is low. A clearer presentation of vibrational population distribution is shown in Figure 4(b), where, to mimic the quantum distribution, we have used a binning procedure of assigning quantum number ν_1 of

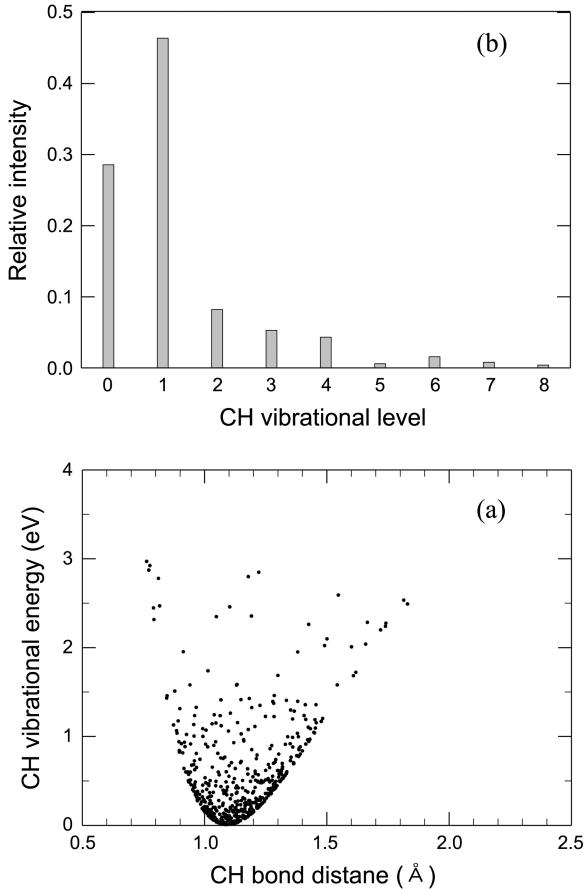

Figure 4. (a) Plot of the CH vibrational energy *vs* the bond distance at 300 K. Each point represents the energy-distance relation at the instant of bond formation. (b) Vibrational population distribution of the CH bond using the data given in (a).

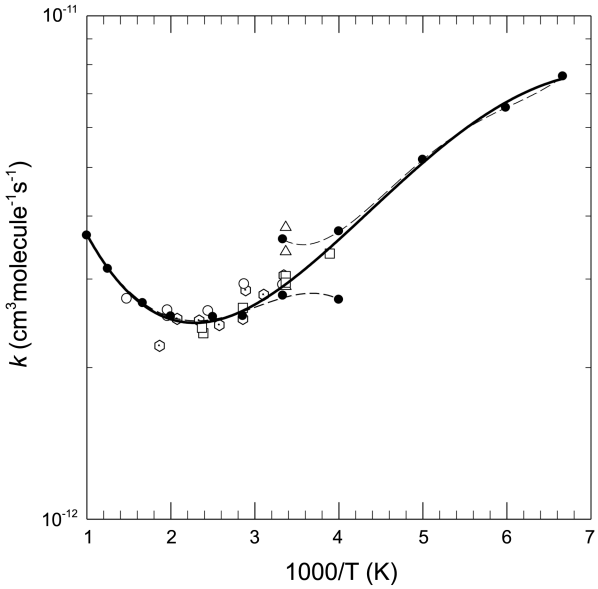

Figure 5. Temperature dependence of the rate constants. The solid curve with filled circles is the present study. Experimental data: hexagons with a dot from Ref. 7, open circles from Ref. 12, open squares from Ref. 10, and open triangles from Ref. 11. The upper dashed curve is for k of the complex-mode model extended to 300 K and the lower dashed curve is for k of the direct-mode model extended to 250 K.

CH_4 corresponding to the computed CH vibrational energy E_{CH} through the relation $\nu_1 = int[E_{CH}/E_{vib}(\nu_1)]$, $E_{vib}(\nu_1)$ being the harmonic-oscillator eigenvalue. The highest distribution appears at $\nu_1 = 1$. The population for $\nu_1 > 4$ is very low, as the reaction system does not have sufficient energy for the production of highly excited CH bond at 300 K.

In Figure 5, we plot the temperature dependence of calculated rate constants over the 150-1000 K range using the complex-mode at T < 300 K and the direct-mode trajectory at T ≥ 300 K. Although emphasis is placed on the low region, we include the higher region to show how the complex-mode model relates to the direct-mode result. The rate constant takes the minimum value of 2.53×10^{-12} at 400 K and increases in both directions as the temperature is varied. It increases to 3.66×10^{-12} at 1000 K and to as large as 7.58×10^{-12} at 150 K. Rate constants are expressed in cm^3 $molecule^{-1}$ s^{-1} throughout the paper. We first note that the high-temperature branch is a thermally activated process and displays positive temperature dependence, approximately paralleling the increase of the mean speed of collision. At temperatures below 300 K, the complex-mode mechanism based on the contribution of attractive interaction leads to strongly negative temperature dependence. Other factors contributing to the dependence are the tunneling of H-atom in the trapped state and the nascent complex returning to the reactant state at a faster rate than going on to the products. The tunneling factor is only 1.48 at 300 K, but increases 2.86 at 150 K. Note that it is only 1.10 at 1000 K. Even without tunneling corrections the ratio k(150K)/k(300 K) is 1.4, because of the importance of molecular attraction. The strength of molecular attraction decreases when the temperature increases as thermal motion tends to destroy the preferred orientation of $H_3C\cdots HBr$, which leads to decrease in the reaction rate. Further, as the temperature increases, some of the incoming trajectories with energy above the barrier tend to hit the repulsive wall on the PES and bounce back to the entrance, which also leads to decrease in the reaction rate. Therefore, the three factors, namely intermolecular attraction, H-atom tunneling and barrier recrossing cause the decrease of the rate constant when the temperature is raised in the complex-mode mechanism (*i.e.*, negative temperature dependence). Above 300 K, where the reaction occur in direct-mode interactions, however, thermal effects overcome these contributions and lead to the rate constant increasing with rising temperature. As shown in Figure 5, the complex-mode interaction seriously overestimates the rate at 300 K, whereas the direction-mode interaction underestimates below 300 K; see dashed lines extending the lower and higher branches.

Over the temperature range of 350-150 K, the variation of logk *vs* 1/T is nearly linear giving an Arrhenius expression $k_{HBr} = 1.10 \times 10^{-12}$ exp(299/T) with a negative activation energy of 2.48 kJ mol^{-1}. The variation between 500 and 1000 K is positive, giving $k_{HBr} = 5.12 \times 10^{-12}$ exp(−366/T), E_{act} = 3.04 kJ mol^{-1}. Although it is slight, the temperature

dependence is negative even in the intermediate range 300-500 K, where the Arrhenius expression is 2.19×10^{-12} exp(66.7/T), E_{act} = 0.554 kJ mol^{-1}. The values of k_{HBr} at intermediate temperatures showing negative temperature dependence are in agreement with experimental data by Seakins *et al*.,[7] Nicovich *et al*.[10] and Seetula:[12] see Figure 5. We note the highest temperature considered by Seakins *et al.*[7] is 536 K, where $k = (2.21 \pm 0.18) \times 10^{-12}$. The upper limit of the latter value is close to the curve calculated in the present study. The Arrhenius fit of the data reported by Seakins *et al.*[7] is $k_{HBr} = (1.57 \pm 0.26) \times 10^{-12}$ exp[(1.6 ± 0.6) kJ mol^{-1}/RT] over the temperature range 299-536 K, whereas that by Nicovich *et al.*[10] is $k_{HBr} = (1.36 \pm 0.10) \times 10^{-12}$ exp[(233 ± 23)/T] for 257-422 K. Seetula's expression reported in Ref. 12 is $k_{HBr} = (2.3 \pm 0.5) \times 10^{-12}$ exp[(0.60 ± 0.17) kJ mol^{-1}/RT] between 299-677 K, where k_{HBr} slightly increases from 510 to 677 K. All measurements show negative activation energy. Also shown in Figure 5 are the measured values by Krasnoperov and Mehta (2.9 ± 0.7), (3.8 ± 1.5) and (3.4 ± 1.3) × 10^{-12} at the buffer gas pressures of 1.05, 11.2 and 101 bar, respectively, at 297 ± 3 K.[11] The latter study is important as it shows the measured rate constant is independent of pressure within the experimental error. We note that in the reactant CH_3 sampled according to the Boltzmann distribution of internal energy states, the ν_1 CH vibration is in the ground state in nearly all trajectories at room temperature. Even at 600 K, 99.96% of the sample is in the ground state. The vibrational population of HBr is similarly distributed in the sample. Thus we find that the occurrence of negative temperature dependence does not come from vibrational excitation of the reactants as previously noted in Ref. 11.

Concluding Comments

Potential energy surfaces constructed for CH_3 + HBr → CH_4 + Br using analytical potential functions show the presence of a shallow attractive well and low energy barrier in the entrance channel. The topology strongly affects the temperature dependence of reaction rates at low temperatures, where a complex-mode collision model in the quasi-classical trajectory approach shows a negative temperature dependence of rate constants below room temperature. The effects of attractive interaction, H-atom tunneling and re-crossing of weakly bound complexes are found to be responsible for the temperature dependence. At intermediate temperatures between 300 and 500 K, the rate constant exhibits a slightly negative temperature dependence. At higher temperatures, thermal effects overcome the attractive interaction and lead to a positive temperature dependence. Rate constants vary from 7.58×10^{-12} at 150 K, to 2.53×10^{-12} at 400 K and then to 3.66×10^{-12} cm^3 molecule^{-1} s^{-1} at 1000 K. Tunneling corrections are important at lower temperatures (2.86 at 150 K) but are insignificant at higher temperatures (1.10 at 1000 K).

The population distribution of ν_1 vibrational energy of the nascent CH bond is peaked at ν_1 = 1. The population of highly excited states ($\nu_1 > 4$) is found to be insignificant as the reaction does not produce sufficient energy for such excitation. The direct-mode reaction at high temperatures occurs on the initial impact, whereas the complex-mode reaction at low temperatures occurs after a long period of $H_3C\cdots HBr$ intermolecular motion. In the complex-mode reaction, HBr dissociation occurs in a series of excitations toward the dissociation threshold,

Acknowlgments. J. Ree gratefully acknowledges the financial support from the Chonnam National University.

Appendix

The overall interaction potential energy is

$$\begin{aligned}U = &\sum_{i=1}^{3} D_i \{\exp[(r_{e,i} - r_i)/a_i] - 2\exp[(r_{e,i} - r_i)/2a_i]\} \\ &+ \sum_{i=1}^{3} D_{HH_m} \{\exp[(r_{e,HH_m} - r_{HH_{m,i}})/a_{HH_m}] \\ &- 2\exp[(r_{e,HH_m} - r_{HH_{m,i}})/2a_{HH_m}]\} \\ &+ \sum_{i=1}^{3} D_{BrH_m} \{\exp[(r_{e,BrH_m} - r_{BrH_{m,i}})/a_{BrH_m}] \\ &- 2\exp[(r_{e,BrH_m} - r_{BrH_{m,i}})/2a_{BrH_m}]\} \\ &+ \sum_{i=1}^{3} D_{CH_m} \{\exp[(x_{e,CH_m} - x_{CH_{m,i}})/a_{CH_m}] \\ &- 2\exp[(x_{e,CH_m} - x_{CH_{m,i}})/2a_{CH_m}]\} \\ &+ \tfrac{1}{2}D_{CBr}\{\exp[(r_{e,CBr} - r_{CBr})/a_{CBr}] + 2\exp[(r_{e,CBr} - r_{CBr})/2a_{CBr}]\} \\ &+ c(e^2/4\pi\varepsilon_o)\{1/[R + \gamma_H(r_{e,HBr} + r_{HBr})] - 1/[R - \gamma_{Br}(r_{e,HBr} + r_{HBr})]\} \\ &- (e\mu_{HBr}/4\pi\varepsilon_o)\cos\Theta/R^2 - (e^2\alpha_{HBr}/8\pi\varepsilon_o)/R^4 - (e^2\alpha_{CH_3}/8\pi\varepsilon_o)/R^4 \\ &- (\alpha_{CH_3}\mu_{HBr}^2/4\pi\varepsilon_o)(3\cos^2\Theta + 1)/R^6, \end{aligned} \quad (A1)$$

where the subscript "e" stands for the equilibrium distance, $\gamma_{H/Br} = m_{H/Br}/(m_H + m_{Br})$, and μ and α are the dipole moment and polarizability of the reactant indicated, respectively. The first sum is for the H-Br, C-H and C-Br interactions. The second sum is for the interactions of H of HBr with each of the methyl hydrogen atoms (three H_m). Similarly, the third sum is the interactions of Br of HBr with the methyl H atoms. The fourth sum is for the intramolecular C-H_m interactions of the methyl radical. An anti-bonding function of the C-Br interaction is introduced to facilitate the removal of fragment Br from the reaction zone. The intramolecular interactions between H_m atoms in the methyl group do not contribute to the reaction process and are not included. The parameter *c* represents a partial ionic character of HBr estimated by $\mu_{HBr}/er_{e,HBr}$. The interatomic distances are

$$r_{CH}/r_{CBr} = \{R^2 + [\gamma_{Br/H}(r_{e,HBr} + r_{HBr})]^2 \mp 2\gamma_{Br/H}(r_{e,HBr} + r_{HBr})R\cos\Theta\}^{1/2}, \quad (A2)$$

$$\begin{aligned} r_{HH_m} = \{&r_{CH'}^2 + [(x_{e,CH_m} + x_{CH_m})\cos(2\pi/3)]^2 + 2(x_{e,CH_m} + x_{CH_m}) \\ &\cos(2\pi/3) r_{CH'} \sin(\theta - \Theta - \chi_H) + [(x_{e,CH_m} + x_{CH_m})\sin(2\pi/3) \\ &- \gamma_{Br}(r_{e,HBr} + r_{HBr})\cos\phi]^2\}^{1/2}, \end{aligned} \quad (A3)$$

$$\begin{aligned} r_{BrH_m} = \{&r_{CBr'}^2 + [(x_{e,CH_m} + x_{CH_m})\cos(2\pi/3)]^2 + 2(x_{e,CH_m} + x_{CH_m}) \\ &\cos(2\pi/3) r_{CBr'} \sin(\theta - \Theta + \chi_{Br}) + [(x_{e,CH_m} + x_{CH_m})\sin(2\pi/3) \\ &+ \gamma_H(r_{e,HBr} + r_{HBr})\cos\phi]^2\}^{1/2}, \end{aligned} \quad (A4)$$

where $\chi_H = \sin^{-1}[\gamma_{Br}(r_{e,HBr}+r_{HBr})\cos\phi\sin\Theta/r_{CH'}]$, $\chi_{Br} = \sin^{-1}[\gamma_H(r_{e,HBr}+r_{HBr})\cos\phi\sin\Theta/r_{CBr'}]$. The distances $r_{CH'}$ and $r_{CBr'}$ take the same expressions as r_{CH} and r_{CBr}, respectively, except that $(r_{e,HBr}+r_{HBr})$ is multiplied by $\sin\phi$. Eqs. (A3) and (A4) are for one of the three methyl hydrogen atoms, say $H_{m,1}$. For $H_{m,2}$ and $H_{m,3}$, the distances can be determined similarly after rotating the $CH_{m,1}$ bond by $2\pi/3$ and $4\pi/3$, respectively, from the YZ plane.

References

1. Andersen, H. C.; Kistiakowsky, G. B. *J. Chem. Phys*. **1943**, *11*, 6.
2. Kistiakowsky, G. B.; Van Artsdalen, E. R. *J. Chem. Phys*. **1944**, *12*, 469.
3. Williams, R. R., Jr.; Ogg, R. A., Jr, *J. Chem. Phys*. **1947**, *15*, 696.
4. Fettis. G. C.; Trotman-Dickenson, A. F. *J. Chem. Soc*. **1961**, 3037.
5. Batt, L.; Cruickshank, F. R. *J. Phys. Chem*. **1967**, *71*, 1836.
6. Russell, J. J.; Seetula, J. A.; Gutman, D. *J. Am. Chem. Soc*. **1988**, *110*, 3092.
7. Seakins, P. W.; Pilling, M. J.; Niiranen, J. T.; Gutman, D.; Krasnoperov, L. N. *J. Phys. Chem*. **1992**, *96*, 9847.
8. Yu, T.; Lin, M. C. *Int. J. Chem. Kinet*. **1994**, *26*, 771.
9. Dobis, O.; Benson, S. W. *J. Am. Chem. Soc*. **1995**, *117*, 8171.
10. Nicovich, J. M.; van Dijk, C. A.; Kreutter, K. D.; Wine, P. H. *J. Phys. Chem*. **1991**, *95*, 9890.
11. Krasnoperov, L. N.; Mehta, K. *J. Phys. Chem. A* **1999**, *103*, 8008.
12. Seetula, J. A. *Phys. Chem. Chem. Phys*. **2002**, *4*, 455.
13. Sheng, L.; Li, Z. S.; Liu, J. Y.; Xiao, J. F.; Sun, C. C. *J. Comput. Chem*. **2004**, *25*, 423.
14. Krasnoperov, L. N.; Peng, J.; Marshall, P. *J. Phys. Chem. A* **2006**, *110*, 3110.
15. Trotman-Dickenson, A. F.; Milne, G. S. *Tables of Bimolecular Gas Reactions*, NSRDS-NBS 9, National Bureau of Standards, Washington, DC, 1967.
16. Chen, Y.; Rauk, A.; Tschuikow-Roux, E. *J. Phys. Chem*. **1991**, *95*, 9900.
17. Seetula, J. A.; Eskola, A. J. *Chem. Phys*. **2008**, *351*, 141.
18. Golden, D. M.; Peng, J.; Goumri, A.; Yuan, J.; Marshall, P. *J. Phys. Chem. A* **2012**, *116*, 5847.
19. McElroy, C. T.; McLinden, C. A.; McConnell, J. C. *Nature* **1999**, *397*, 338.
20. Lary, D. J. *J. Geophys. Res*. **1996**, *101*, 1505.
21. Platt, U.; Allan, W.; Lowe, D. *Atmos. Chem. Phys*. **2004**, *4*, 2393.
22. Keil, A. D.; Shepson, P. B. *J. Geophys. Res*. **2006**, *111*, D17303.
23. Liao, J.; Huey, L. G.; Scheuer, E. *et al. Atmos. Chem. Phys*. **2012**, *12*, 1327.
24. Hydrogen bromide, Chapter 6, p. 43. Available at http://archive.defra.gov.uk/environment/quality/air/air-quality/publications/halogens/chapter 6. Accessed April 26, 2013.
25. Ree, J.; Kim, Y. H.; Shin, H. K. *Int. J. Chem. Kinet*. **2011**, *43*, 455.
26. Blanksby, S. J.; Ellison, G. B. *Acc. Chem. Res.* **2003**, *36*, 255.
27. Eckart, C. *Phys. Rev.* **1930**, *35*, 1303.
28. Wigner, E. *Z. physik. Chem.* (Leipzig) **1932**, *B19*, 203.
29. Bell, R. P. *Proc. Roy. Soc.* (London) **1933**, *139*, 466.
30. Bell, R. P. *Tans. Faraday Soc.* **1959**, *55*, 1.
31. Shavitt, I. *J. Chem. Phys*. **1959**, *31*, 1359.
32. Shin, H. K. *J. Chem. Phys*. **1963**, *39*, 2934.
33. Zuev, P. S.; Sheridan, R. S.; Albu, T. V.; Truhlar, D. G.; Hrovat, D. A.; Borden, W. T. *Science* **2003**, *299*, 867.
34. Moss, R. A.; Sauers, R. R.; Sheridan, R. S.; Tian, J.; Zuev, P. S. *J. Am. Chem. Soc.* **2004**, *126*, 10196.
35. McMahon, R. J. *Science* **2003**, *299*, 833.
36. Landau, L. D.; Lifshitz, E. M. *Quantum Mechanics*; Pergamon 1958; pp 171-178.
37. IMSL MATH/LIBRARY, Fortran Subroutines for Mathematical Applications, Version 2.0, IMSL, Houston, TX, 1991, pp 755-771 for DIVPAG to solve an initial-value problem for ordinary differential equations using Adams-Moulton's method and pp. 1319-1320 for DRUN to generate random numbers from flat (0,1) distributions.
38. Akin, F. A.; Ree, J.; Ervin, K. M.; Shin, H. K. *J. Chem. Phys*. **2005**, *123*, 064308.
39. Su, J. Z.; Teitelbaum, H. *Int. J. Chem. Kinet*. **1994**, *26*, 159.
40. Hirschfelder, J. O.; Curtiss, C. F.; Bird, R. B. *Molecular Theory of Gases and Liquids*; John Wiley & Sons: 1967; p 1200.
41. Shin, H. K. *J. Chem. Phys.* **1967**, *47*, 3302.
42. Werner, H.-J.; Rosmus, P. *J. Chem. Phys*. **1980**, *73*, 2319.
43. Jin, P.; Brinck, T.; Murray, J. S.; Politzer, P. *Int. J. Quantum Chem*. **2003**, *95*, 632.
44. Fernandez, B.; Coriani, S.; Rizzo, A. *Chem. Phys. Lett*. **1998**, *288*, 677.
45. Huber, K. P.; Herzberg, G. *Constants of Diatomic Molecules*, Van Nostrand Reinhold, New York, 1979.
46. Shimanouchi, T. ed., *Tables of Molecular Vibrational Frequencies*, Consolidated Vo1. I, NSRDS-NBS 39, National Bureau of Standards, Washington, DC, 1972.
47. Herzberg, G. *Electronic Spectra and Electronic Structure of Polyatomic Molecules*, Van Nostrand, New York, 1966.
48. Huang, Z.-H.; Guo, H. *J. Chem. Phys*. **1992**, *97*, 2110.
49. Pamidimukkala, K. M.; Rogers, D.; Skinner, G. B. *J. Phys. Chem. Ref. Data* **1982**, *11*, 83.
50. Robertson, S. H.; Wardlaw, D. M.; Hirst, D. M. *J. Chem. Phys*. **1993**, *99*, 7748.